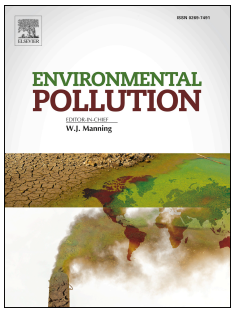

Multi-omics analysis revealed NMBA induced esophageal carcinoma tumorigenesis via regulating PPARα signaling pathway

Hu Zhang, Chao Zhao, Ying Zhanga, Lu Lu, Wei Shi, Qian Zhou, Yuepu Pu, Shizhi Wang, Ran Liu, Lihong Yin

PII: S0269-7491(23)00371-8

DOI: https://doi.org/10.1016/j.envpol.2023.121369

Reference: ENPO 121369

To appear in: *Environmental Pollution*

Received Date: 7 December 2022

Revised Date: 13 February 2023

Accepted Date: 26 February 2023

Please cite this article as: Zhang, H., Zhao, C., Zhanga, Y., Lu, L., Shi, W., Zhou, Q., Pu, Y., Wang, S., Liu, R., Yin, L., Multi-omics analysis revealed NMBA induced esophageal carcinoma tumorigenesis via regulating PPARα signaling pathway, *Environmental Pollution* (2023), doi: https://doi.org/10.1016/j.envpol.2023.121369.

Authorship contribution statement

Hu Zhang: Conceptualization, Software, Data analysis, Writing-Original draft preparation and Editing. Chao Zhao: Methodology. Ying Zhang: Validation. Lu Lu: Visualization. Wei Shi: Software. Qian Zhou: Conceptualization. Shizhi Wang: Supervision. Ran Liu: Writing- Reviewing. Yuepu Pu: Supervision. Lihong Yin: Writing- Reviewing, and Supervision.

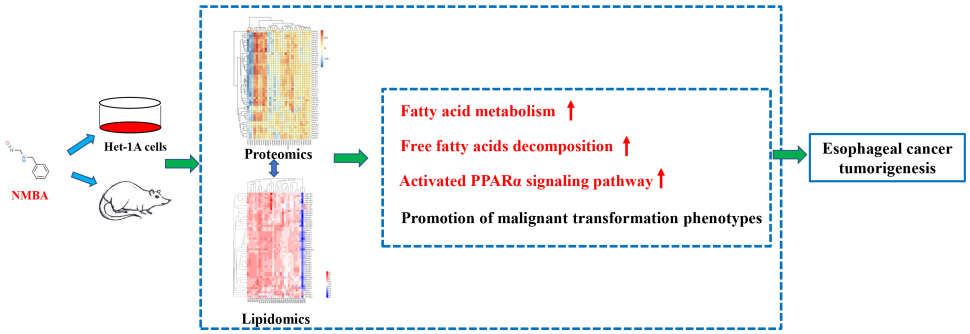

Multi-omics analysis revealed NMBA induced esophageal carcinoma tumorigenesis via regulating PPARα signaling pathway

Hu Zhang[a] . Chao Zhao[b]. Ying Zhang[a] . Lu Lu[a]. Wei Shi[a]. Qian Zhou[a] . Yuepu Pu[a]. Shizhi Wang[a], Ran,Liu[a] . Lihong Yin[a*]

[a] Key Laboratory of Environmental Medicine Engineering, Ministry of Education, School of Public Health, Southeast University, Nanjing 210009, People's Republic of China

[b] School of Nursing & School of Public Health, Yangzhou University, Yangzhou 225000, China

* Correspondence Author

Lihong Yin, School of Public Health, Southeast University, Nanjing, 210009, People's Republic of China

Tel: +86-025-8327-2583

Fax: +86-025-8327-2583

Email: lhyin@seu.edu.cn

Abstract:

As widespread environmental carcinogens causing esophageal carcinoma (EC), the effects of N-nitrosamines on human health hazards and accurate toxicity mechanisms have not been well-elucidated. In this study, we explored the tumorigenic mechanism of N-nitrosomethylbenzylamine (NMBA) exposure using both cell and rat models. It was found that NMBA (2 μM) exposure for 26 weeks induced malignant transformation of normal esophageal epithelial (Het-1A) cells. After then proteomics analysis showed that lipid metabolism disorder predominantly participated in the process of NMBA-induced cell malignant transformation. Further the integrated proteomics and lipidomics analysis revealed that the enhancement of fatty acid metabolism promoted the EC tumorigenesis induced by NMBA through facilitating the fatty acid-associated PPARα signaling pathway. The animal studies also revealed that accelerated fatty acid decomposition in the progression of NMBA-induced EC models of rats was accompanied by the activation of the PPARα pathway. Overall, our findings depicted the key dynamic molecular alteration triggered by N-nitrosamines, and provided comprehensive biological perspectives into the carcinogenic risk assessment of N-nitrosamines.

Keywords: NMBA; esophageal carcinoma; fatty acid metabolism; PPARα pathway

1. Introduction

As organic compounds with the chemical structure R_2N-N double bond O, N-nitrosamine compounds formed by the reaction of nitrite preparations with secondary amines have been detected in drinking water, cosmetics, artificial foods and cigarette smoke. (Sambiagio et al., 2022; Tang et al., 2022; Trejo-Martin et al., 2022). As well-known mutagen precursors, numerous N-nitrosamines were classified as carcinogenic mutagens and potent rodent carcinogens (Li and Hecht, 2022; Vogel and Norwig, 2022). N-nitrosodiethylamine (NDEA) and N-nitrosodimethylamine (NDMA) have been classified as possibly carcinogenic to humans by the IARC (Abdullah et al., 2022). Epidemiological evidences have demonstrated that the nitrates, nitrites and N-nitroso compounds exerted strong potential relationship with esophagus cancer, gastric cancer, colorectal cancer and other digestive carcinogenic risk (Boetzel et al., 2022; Li et al., 2022b; Liu et al., 2022a). The presence of N-nitrosamines and their precursors in drinking water and food was critical to ensuring public health (Choi et al., 2022; Li et al., 2022). The World Health Organization (WHO) has set a guideline value of 100 ng/L for NDMA commonly detected in drinking water (Cai et al., 2023). In the United States, California has set a limit of 10 ng/L for NDMA, NDEA and N-nitrosopropylamine (NDPA) in drinking water. According to the Environmental Protection Agency (EPA), the levels of NMBA exposure in most areas of the United States were generally low, with concentrations of 0.1 μg/L or less. However, in certain areas, NMBA exposure levels could reach up to 1.5 μg/L (Ferrer et al., 2010). In China, approximately 29% of

tap water samples have detected the concentration of NDMA higher than 10 ng/L, and some tap water was even greater than 40 ng/L (Qiu et al., 2021). The EPA has set health reference levels for NMBA (30 ng/L), NDEA (0.4 ng/L), NDMA (0.6 ng/L) (EPA, 2016). To date, the controlling the formation of N-nitrosamines and removing them to satisfactory levels were challenging. N-nitrosamine compounds may cause adverse health problems on account of the mutagenic, teratogenic and carcinogenic potential (Liao et al., 2022; Maqbool et al., 2021; Zhao et al., 2020).

Esophageal cancer (EC) is currently one of the pernicious tumors of the digestive system, with the mortality rate ranking sixth in the world and the incidence rate ranking fourth in China (Chen et al., 2016; Sung et al., 2021). The occurrence and development of EC were caused by the integration of factors such as heredity, environment, and lifestyle, among which environmental risk factors led to the key regulatory mechanisms and sensitive biomarkers for the progression of EC (Hagi et al., 2022; Luo et al., 2021; Xia et al., 2022). Studies have suggested that the people in high-risk areas of EC were exposed to higher levels of N-nitrosamines, and endogenous exposure to N-nitrosamines was involved in the EC tumorigenesis in the high incidence areas of China (Zhao et al., 2019a; Zhao et al., 2020; Zhao et al., 2019b). The current researches mainly focused on the gene expression differences or genotoxic damage induced by N-nitrosamines, there was lack of the studies on the dynamic molecular destabilization in the systematic and comprehensive explanation of the health hazards of EC caused by N-nitrosamines (Dong et al., 2022; Gao et al., 2022; Molina-Aguilar et al., 2022).

Multi-omics technology was helpful to ascertain metabolic changes in numerous

diseases induced by environmental exposure (Lee et al., 2021; Xu et al., 2020). The integration of multi-omics could effectively capture multi-faceted networks from genes to phenotypes, which may be available to provide direct evidence for describing the complex biochemistry of cells and elucidate a range of molecular toxicity mechanisms after exposure to environmental pollutants (Shen et al., 2022; Yan et al., 2022; Zhang et al., 2022a). The integration of metabolomic and lipidomic analysis unveiled that the dysfunction of unsaturated fatty acids metabolism pathway primarily participated in the malignant transformation of Het-1A cells induced by N-methyl-N'-nitro-N-nitrosoguanidine (MNNG) (Zhang et al., 2022b). Multi-omics analysis showed a strong correlation between abnormal lipid metabolism and residual micropollutants (semivolatile organic compounds and N-nitrosamines) induced by long-term UV effluent exposure (Deng et al., 2022). Therefore, the overall multi-omics analysis was conducive to emphasize the dynamic molecular mechanism of esophageal carcinoma caused by N-nitrosamines exposure.

N-nitroso-N-methylbenzylamine (NMBA) was identified from food and human stomach contents collected from Linxian, an esophageal carcinoma high-incidence area in China (Cui et al., 2022). The average levels of volatile nitrosamines and NMBA in dietary samples detected in the high incidence of EC in China were 312.0 μg/kg, and the daily intake of N-nitrosamines was 286.5 μg/day (Lin et al., 1997; Lu et al., 1991). Oncogenic activation of NBMA was generally believed to occur through P450-catalyzed hydroxylation of methylene groups in esophageal microsomes, and NMBA-induced lesions at various pathological stages during the development of rat esophageal

cancer were histologically similar to human EC (Cui et al., 2020; Yang et al., 2012). Epidemiological studies in the areas with high incidence of esophageal cancer in China have reported that the environmental carcinogens NMBA and the deficiency of riboflavin (RBF) may be central risk factors for esophageal cancer (Pan et al., 2019). So far, there were few reports on the molecular mechanism of NMBA-induced esophageal carcinogenesis. In this study, we constructed the NMBA-induced cell malignant transformation model of Het-1A cells, subsequently, multi-omics analysis was firstly applied to illustrate the novel toxicological mechanism of malignantly transformed cells provoked by NMBA, which comprehensively investigated the regulation mechanism of lipid metabolism disturbance in the Het-1A cells malignant transformation induced by N-nitrosamines, and the results were further verified in the rat EC models induced by NMBA. In all, our study extensively mapped the regulatory network and mechanism of lipid metabolism disorder involved in the toxic effects of esophageal cancer caused by N-nitrosamines, which exerted great significance for discovering the early biomarkers and intervention targets of nitrosamines-induced EC tumorigenesis.

2. Materials and methods

2.1. Chemicals and reagents

NMBA was provided by Nanjing University (Nanjing, China) and was found to be > 95% purity by LC-MS/MS (Zhao, et al., 2022). The LC/MS-grade methyl tert-butyl ether (MTBE), methanol (MeOH), acetonitrile (ACN) and isopropanol (IPA) were

procured from Merk (Darmstadt, Germany). The free fatty acids (FFAs) mixture containing dodecanoic acid (FFA 12:0), myristic acid (FFA 14:0), palmitic acid (FFA 16:0), palmitoleic acid (FFA 16:1), oleic acid (FFA 18:0), linoleic acid (FFA 18:1), y-linoleic acid (FFA 18:3), arachidonic acid (FFA 20:4), eicosapentaenoic acid (FFA 20:5) and docosahexaenoic acid (FFA 22:6) were obtained from ANPEL Laboratory Technologies (Shanghai, China). The dimethyl sulfoxide (DMSO), palmitic acid-d31(FFA 16:0-d31) and lipid internal standards (IS) 15:0–18:1(d7) PA, 15:0–18:1(d7) PE, 15:0–18:1(d7) PS, 15:0–18:1(d7) PG, 15:0–18:1(d7) PC, 15:0–18:1(d7) PI, 18:1(d7) LPC, 18:1(d7) LPE, 15:0–18:1(d7)-15:0 TG, 18:1(d7) Chol Ester, 18:1(d7) MG, 15:0–18:1(d7) DG, 18:1(d9) SM were applied by Sigma-Aldrich (Bellefonte, PA, USA). The formic acid and ammonium formate were obtained from Merck (Darmstadt, Germany). The Millipore-Q pure system was used to produce ultra-pure water (Synergy UV, Bedford, MA).

2.2. Cell culture and NMBA treatment

The Het-1A cells and EC109 cells were provided by the Chinese Academy of Sciences Cell Bank (Shanghai, China). The Het-1A and EC109 cells were cultured in DMEM medium (Gibco, USA) and RPMI-1640 medium (Gibco, USA) complemented with 10% fetal bovine serum (FBS) and 1% antibiotics (penicillin- streptomycin, Gibco, USA) in an incubator at 37 ℃ with 5% CO_2. The NMBA was dissolved in DMSO and obtained the stock solution at a concentration of 1 mol/L, which was afterwards diluted to 2 μmol/L with DMEM culture medium. For the NMBA exposure, the Het-1A cells of 80% confluent were exposed to NMBA (2 μmol/L) or solvent control (DMSO) for 24 hours,

once per passage. The environmental exposure dose of NMBA was selected from our previous work (Zhang et al., 2022c), and the exposure concentration was close to the human urine exposure levels of N-nitrosamines (Ferrer et al., 2010; Hu et al., 2016; Zhao et al., 2020). As for the inhibitory effect assays, the P40 passage malignant transformed cells were pretreated with or without PPARα pathway inhibitor (GW6471, 10 μM) for 48 h.

2.3. Cell proliferation assay

The cell viability was examined by the CCK8 (Cell Counting Kit-8) assay. The P0, P10, P20, P40 generation of malignant transformed cells and their solvent control were seeded into a 96-well plate at a density of 8000 cells/well, the CCK8 reagent was added into wells and incubated at 37 ℃ for 1 h. The OD values were detected at 450 nm wavelength with Multiskan SkyHigh (Thermo Fisher Scientific, USA).

2.4. Transwell assay

The 24-well Mill cell chamber (corning 3422) was applied to detect cell invasion and migration capacity. After the cells collected, the upper chambers were seeded 2×10^5 cells with serum-free DMEM medium. The 15% FBS–DMEM medium was filled in the lower chamber and incubated for 24 h. The cells on the top membrane surface were wiped, then the chambers were fixed with 95% ethanol and stained with 0.1% crystal violet. Subsequently, the cells were counted under the light microscope (Zeiss, Karl, Germany). The migration assay was performed in a homogeneous method without the Matrigel coating.

2.5. Reverse transcription-quantitative (RT-q) PCR

The total RNA of cells and tissues was extracted using the Trizol Reagent (Invitrogen, USA) in line with the manufacturer's protocols. Reverse transcription of RNA was performed using the PrimeScript RT kit (Takara, Japan), and qPCR quantification was performed using TB Green Premix Ex Taq II (Takara, Japan). The relative mRNA levels were determined by the $2^{-\Delta\Delta Ct}$ method and internal control was applied normalizing as β-actin. The gene primers were listed in Table S1.

2.6. Western blot analysis

The cells and tissues (50 mg) were isolated in ice-cold RIPA buffer (Beyotime, China). The proteins were separated using 10% SDS-PAGE and electroblotted onto a polyvinylidene fluoride (PVDF) membrane (Immobilon®-P) after quantitative determination of the protein concentration. The membranes were blocked in 5% non-fat milk for 1 h, then incubated overnight at 4 ℃ with primary antibodies anti-PPARα (1:1000, Abcam), anti-CD36 (1:2000, Abcam), anti-CPT1 (1:2000, Abcam), anti-SCD (1:1000, Abclonal), anti-ACAA2 (1:1000, Abcam), anti-ACBP (1:1000, Abcam), anti-E-cadherin (1:1000, Abcam), anti-N-cadherin (1:1000, Abcam), anti-α-SMA (1:2000, Abcam), anti-Snail (1:2000, Cell Signaling Technology), anti-Vimentin (1:2000, Abcam) and anti-β-actin (1:2000, Cell Signaling Technology). Subsequently, the secondary antibodies (anti-mouse/anti-rabbit) were applied incubating membranes at room temperature for 2 h and protein bands were detected with the Super Signal Kit (Thermo Fisher Scientific, USA).

2.7. Proteomics analysis

The cell samples were dissolved with 200 μL lysis buffer and boiled for further

ultrasonicated. Proteomic sequencing and analysis were conducted by Shanghai Bioprofile Technology (Shanghai, China). Undissolved cellular debris was removed at 4 ℃, 16000 g for 15 min to obtain the supernatant for protein quantification (BCA Protein Assay Kit,Bio-Rad, USA). After protein digestion, 200 μL of buffer ammonium bicarbonate (100 mM) was added to the beads in the filter box, ammonium bicarbonate buffer with trypsin at the enzyme-to-protein ratio of 1:50 was appended into the sample and incubated at 37 ℃ for 20 h. The peptides were loaded onto a the C18-reversed phase column (15 cm long, 75 μm ID, 2 μm, Dr. Maisch GmbH, Ammerbuch, Germany) at a flow rate of 300 nL/min over 60 min. Mass spectrometry parameters and liquid linear gradient conditions were specified in Table S2.

The MS data were analyzed for data explanation and protein annotation against the human database from Uniprot (https://www.uniprot.org). All peptides, proteins and peptide-spectrum matches were filtered with <1% false discovery rate. Hierarchical clustering at the protein or locus level integrated the expression data for analysis. To interpret the sequences, information was extracted from UniProtKB/Swiss-Prot, Kyoto Encyclopedia of Genes and Genomes (KEGG) and Gene Ontology (GO) analysis. The Fisher's exact test was used to perform GO and KEGG enrichment analyses, and FDR correction for multiple testing was also conducted. The STRING database with the Cytoscape software was applied to establish protein–protein interaction (PPI) networks.

2.8. Lipidomics analysis

2.8.1. Lipid extraction and instrumental analysis

The cell and serum samples were homogenized for lipid extraction according to our

previous work (Zhang et al., 2022b; Zhang et al., 2022c). Briefly, the samples were collected and washed with pre-cooled PBS, then added 400 μL methanol/H_2O (3:1, v/v) for protein precipitation. 1 mL of MTBE was added into the mixture and vortex for 30 min at room temperature, 200 uL of deionized water was added for liquid phase separation. The mixture was equilibrated on ice and the supernatant was obtained by centrifugation (14000 g, 15 min, 4 ℃). The organic supernatant was re-dissolved with 200 μL ACN/IPA/H_2O (65:30:5, v/v/v) including 5 μg/mL of IS mixture for instrument analysis. The quality control (QC) sample was generated by collecting 5 μL of each sample. As for LC-MS analysis, the lipid profile analysis was performed using a SCIEX Triple TOF 5600 system (SCIEX, USA) with a Waters ACQUITY UPLC BEH C18 column (1.7 μm particles, 2.1 mm × 50 mm, Waters, Milford, MA). The detailed liquid linear gradient conditions and MS parameters were listed in Table S3.

2.8.2. Targeted free fatty acids analysis

The free fatty acids extraction was conducted using the above lipid separation methods. After re-dissolving with 200 μL ACN/IPA (7:3, v/v), the IS FFA 16:0-d31 (2 μg/mL) was added into each sample for analysis. The multiple reaction monitoring (MRM) analysis was applied to perform LC-MS data acquisition with m/z mass range 100–500, the liquid gradient conditions were consistent with the above lipid profiling methods.

2.8.3. Data processing and analysis

The XCMS online platform was utilized to process the LC-MS/MS raw data acquisition. After peak detection, retention time correction, the metabolite features with missing values in more than 20% of the samples were excluded and QC standard deviations

(RSD) more than 30% were removed out. The data were imported into the SIMCA-P (Umetrics, Sweden) software, then the metabolic differences between different groups were assessed by Principal Component Analysis (PCA) and Orthogonal partial least squares discriminant analysis (OPLS-DA) models. The following data screening criteria were used to select variant metabolites: VIP value >1.5 and the alterations in the features of different groups were statistically significant ($p < 0.05$). The $[M + H]^+$ and $[M – H]^-$ ion adducts were positive and negative acquisition ions, respectively. The peak intensities were normalized by IS and compared to the identified altered metabolites. The differential metabolites were putatively annotated matching the HMDB database and lipidmaps database based on the m/z mass value with tolerance set as 5 ppm and MS^2 spectra. The variant metabolic pathways were enriched with MetaboAnalyst online (http://www.metaboanalyst.ca/) based on KEGG pathway.

2.9. Multi-omics integrated analysis

The integrated proteomics and lipidomics analysis were utilized to calculate the correlation coefficients between the substantially variant metabolites and the related-differential proteins with spearman correlation analysis. The results were further analyzed using R 4.0.1 and Cytoscape tools, including matrix heatmap analysis, hierarchical clustering analysis and correlation network analysis, to explore the interaction relationship between proteinases and lipid metabolites from multiple perspectives.

2.10. Animal model of NMBA exposure

The NMBA-induced esophageal carcinoma rat model was established by our study

group (Zhao et al., 2022). In short, the male F344 rats were intraperitoneally injected into the model group (NMBA, 0.4 mg/kg) and the control group (saline containing 0.05% DMSO) for 3 months. The dosage of rat exposure was selected from the environmental N-nitrosamine internal exposure levels (Zhang et al., 2020; Zhao et al., 2020; Zhao et al., 2022). Esophageal lesions at diverse stages were collected for histological examination and quantitative analysis according to the previous studies (Zhang et al., 2022c). The rat serum was centrifuged at 8000 rpm for 5 min at 4 ℃, then collected and stored at -80 ℃. The Animal Care and Use Committee of Southeast University approved the animal protocols following the ARRIVE guideline.

2.11. Statistical analysis

The data statistical analysis was performed using the SPSS version 24.0 and GraphPad Prism 8.1 software. The Shapiro-Wilk test was used to detect the normality of data distribution of each group. The significant difference between two groups was implemented using the student's t test. One-way analysis of variance (ANOVA) followed by Dunnett's post hoc test was conducted to perform the statistical differences among different groups. The Benjamini-Hochberg false discovery rate (FDR)-adjusted p value < 0.05 was considered as the threshold of statistical significance. All data were displayed as mean ± standard deviation (SD).

3. Results

3.1. NMBA exposure induced Het-1A cells malignant transformation and tumorigenesis

To explore the tumorigenic effect of NMBA exposure and the underlying molecular mechanism, we conducted chronic cell malignant transformation assay by continuously exposing Het-1A cells to environmental exposure levels of NMBA (2 μM) for 26 weeks. As the number of infected generations increased, the cell morphology of the NMBA-exposed group changed from a small, round pavement-like and appositional growth state to an increased volume, pseudopod and irregularly drawn loose state (P40 generation cells) (Fig. S1A). The CCK8 results revealed that the NMBA-exposed cells showed elevated trend accompanied by the increasing infected passages, and the proliferation activity of P40 generation (Pmag) cells was elevated dramatically compared with the control group (Fig. 1A). Also, the western blot analysis of Epithelial-Mesenchymal Transition (EMT) signaling pathway proteins reflecting the degree of cell malignant transformation showed that the expression levels of N-cadherin, Snail, α-SMA and Vimentin were up-modulated with the increasing passages; the level of E-cadherin showed downregulated tendency. Especially, the protein levels in EC109 cells (positive control) were consistent with the trend of the expression in Pmag cells (Fig. 1B). Furthermore, the invasive and migratory capacity of cells were markedly elevated following the chronic NMBA stimulation (Fig. S1B-C). The colony formation assay revealed that the capacity of colony formation was remarkably reinforced along with the increasing generations (Fig. 1C, Fig. S1D). To further examine the effect of malignant transformed cells on tumor growth in vivo, The Pmag cells, positive control (EC109 cells) and the solvent control cells were injected into BALB/c nude mice. The results revealed that the control cells did not produce any xenograft tumors in nude

mice (0 tumor from 6 to injected mice), whereas the mice injected with Pmag cells and EC109 cells appeared bigger tumors (Fig. 1D). In addition, the H&E staining and immunohistochemistry for Ki-67 results revealed that tumor tissues in the NMBA exposure and EC109 groups manifested as similar tumor cell properties (Fig. 1E).

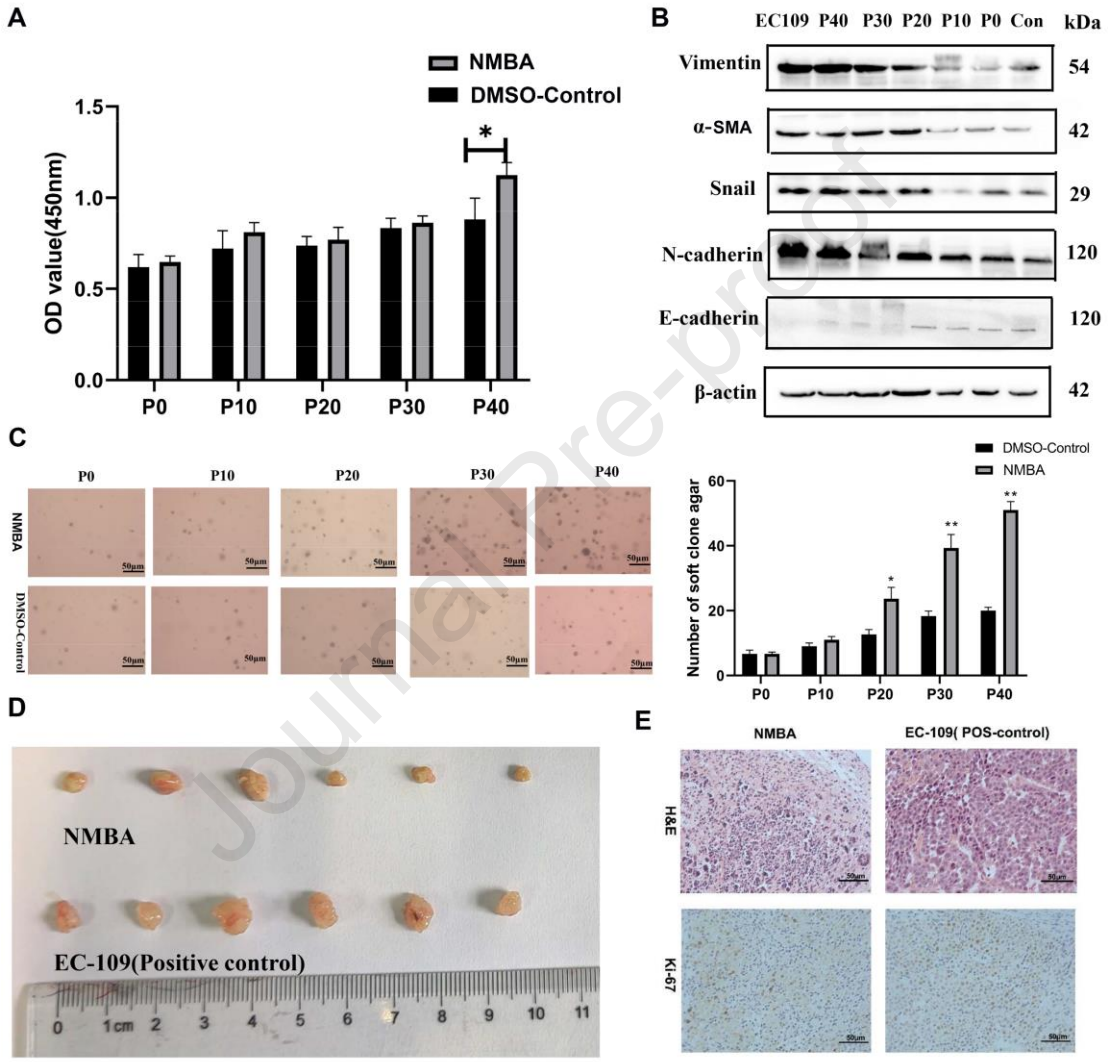

Fig. 1. NMBA exposure induced malignant transformation of Het-1A cells. (A). Proliferative capacity of cells at different stages of malignant transformation. (B). The protein levels of EMT signaling pathway in different generation cells. (C) The soft agar colony formation of different generation cells (bar= 50 μm). (D). NMBA-exposure-transformed cells and positive control cells showed stronger tumorigenicity in nude mice. (E). The H&E staining and Ki67 immunohistochemistry of xenografts (bar= 50

μm). The data were expressed as mean ± SD. *p < 0.05, **p < 0.01.

3.2. Proteomic changes in different stages of malignant transformation cells induced by NMBA

In the present study, to explore the mechanisms between diverse passages (P10, P20, P30, P40) of malignant transformed cells and control cell group (P0), a 4D-label free quantitative proteomics approach was carried out to identify proteomic biomarkers. The scoring plots of PCA modes exhibited apparent separation between the various stages of NMBA-exposed malignant transformed cells (P10, P20, P30 and P40) and the control group (Pcon) (Fig. 2A). In the current experimental conditions, a total of 5894 proteins were identified. The results of subcellular localization showed that the majority of proteins were mainly distributed in cytoplasm (36.1%), membrane (22.74%) and extracellular region (10.81%) (Fig. 2B), which suggested a strong relationship between regulatory lipid metabolites and differential proteins (Lyon et al., 2021; Yang et al., 2021). The KEGG-enrichment analysis revealed that the screened protein biomarkers were also enriched in Ribosome and Ribosome biogenesis in eukaryotes (Fig. 2C). Among these proteins, the expression levels of 199, 282, 389 and 384 proteins were markedly changed under P10, P20, P30 and P40 passage NMBA-exposed cells and displayed as volcano plots (Fig. 2D). Intriguingly, the Venn analysis uncovered that 29 significantly differential proteins aggravated the metabolic disorders on the lipid proteases and mainly enriched in lipid fatty acid metabolism (Fig. 2E, Table S4). Furthermore, we enriched the perturbed lipoprotein-regulated metabolic pathways

based on the KEGG pathway, and these differential metabolic pathways were primarily distributed in PPAR signaling pathway, sphingolipid metabolism, fatty acid degradation, biosynthesis of unsaturated fatty acids metabolism, inositol phosphate metabolism, alpha-linolenic acid metabolism, glycerolipid metabolism and arachidonic acid metabolism (Fig. 2F), implying that dysregulation of lipid fatty acid metabolism participated in NMBA-induced protein profile differences in the progression of Het-1A cells malignant transformation.

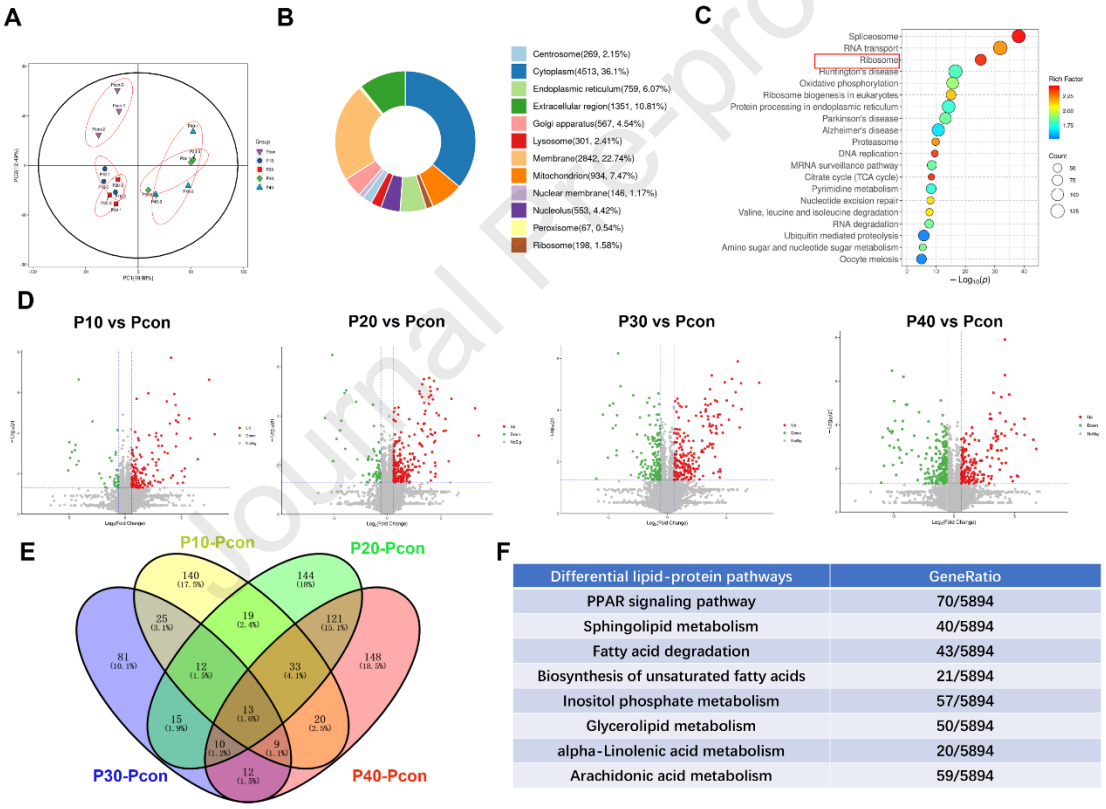

Differential lipid-protein pathways	GeneRatio
PPAR signaling pathway	70/5894
Sphingolipid metabolism	40/5894
Fatty acid degradation	43/5894
Biosynthesis of unsaturated fatty acids	21/5894
Inositol phosphate metabolism	57/5894
Glycerolipid metabolism	50/5894
alpha-Linolenic acid metabolism	20/5894
Arachidonic acid metabolism	59/5894

Fig. 2 Proteomics analysis of cells treated with NMBA. (A). The score plots of PCA model. (B, C). Subcellular localization and KEGG-enrichment analysis. (D). The volcano plots of NMBA-exposed cells compared to the control group. (E). The Venn analysis of differential proteins in cells. (F). The lists of differential lipid-protein pathways.

358

359

360

361 3.3. The cells lipidomic profiling analysis

362 Following the results of proteomic analysis, the cell lipidomic profiles were
363 systematically detected in order to further delineate the dysfunction of lipid metabolism
364 during the Het-1A cells malignant transformation induced by NMBA. The scoring plots
365 of PCA and OPLS-DA models for both positive and negative modes showed
366 pronounced separation between diverse passages of NMBA-exposed groups and
367 control group, suggesting the clustering of different cell groups and demonstrating good
368 model fit and predictive performance (Fig. 3A, B and Fig. S2A, B). Furthermore, the
369 validation of the models was evaluated with 200-time permutation tests and the results
370 indicated good predictability ($Q^2 < 0$, Fig. S2C, D). A total of 140 and 142 lipids with
371 VIP value > 1.5 were putatively retained in positive and negative ion modes. After one-
372 way ANOVA test for univariate data analysis was employed to identify the most
373 remarkably variant lipids, the 55 differential lipid markers were annotated and listed in
374 Table S5. The abnormal lipid metabolites were primarily consisted with free fatty acids
375 (FFA), phosphatidylcholines (PC), phosphatidic acids (PA), phosphatidylserines (PS),
376 phosphatidylethanolamines (PE), phosphatidylglycerols (PG), sphingomyelins (SM),
377 lyso-phosphatidylethanolamines (LPE) and cholesterols (CE). Pathway enrichment
378 analysis using MetaboAnalyst (5.1) showed that perturbed lipid biomarkers were
379 mainly enriched in biosynthesis of unsaturated fatty acids metabolism,
380 glycerophospholipid metabolism, linoleic acid metabolism and arachidonic acid

metabolism (Fig. 3C). Hierarchical clustering analysis was performed to detect the relative expression levels of differential lipid markers, the heatmap analysis showed that the most lipid metabolites revealed attenuated trend along with the increasing passages of malignant transformed cells induced by NMBA (Fig. 3D), In particular, the most significant differences in free fatty acids (FFA) uncovered the acceleration of fatty acid catabolism during the cell malignant transformation, further demonstrating the involvement of fatty acid metabolism disorders in the process of NMBA exposure-induced Het-1A cells malignant transformation.

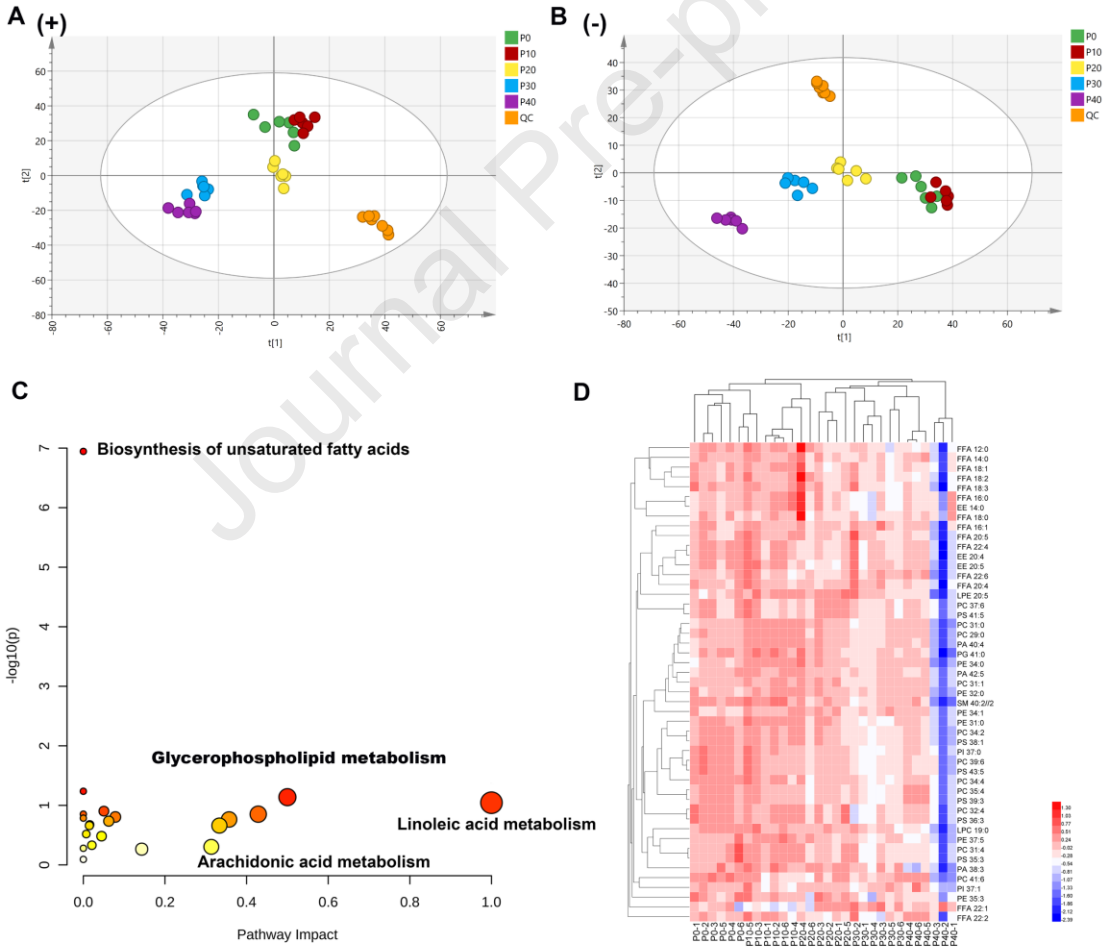

Fig. 3. The lipidomic profiles of malignant transformed cells. (A, B). The score plots of positive OPLS-DA model ($R^2Y = 0.945$, $Q^2 = 0.746$) and negative OPLS-DA model ($R^2Y = 0.973$, $Q^2 = 0.744$) in cells. (C). The metabolic pathways of differential lipids.

(D). Hierarchical clustering analysis of altered lipid markers.

3.4. Integrated analysis of cell proteomics and lipidomics

In order to interpret the role of key differential proteins in the regulation of altered lipid homeostasis, the integrative analyses of proteomics and lipidomics on NMBA-treated Het-1A cells were applied to evaluate the association. The results of correlation coefficient matrix heatmap analysis showed that the majority of lipid metabolites were negatively correlated with the perturbed proteins (Fig. 4A). To visualize the similarities and differences in the expression patterns of markedly differential proteins and aberrant metabolites, the Spearman correlation hierarchical clustering analysis was performed and presented in the form of correlation hierarchical clustering heatmap, the results revealed that P16671 (CD36)，O00767 (SCD) and P50416 (CPT1) were negatively and Q01469 (FABP5), P42765 (ACAA2), Q9NYP7 (ELOVL5), O43772 (SLC25A20), P33121 (ACSL1) and Q8NEB9 (PIK3C3) positively associated with most lipid metabolites, especially FFAs (Fig. 4B). The expression of omics clustering heatmap analysis showed increased trend in critical differential protein expression and revealed declined tendency in lipid free fatty acids between the increasing passages of NMBA-exposed malignant transformed cells (P10, P20, P30 and P40) and the control group (Fig. 4C). Moreover, the correlation analysis network exhibited the close regulation effects between CD36, SCD, CPT1, ACBP, ACAA2 and differential free fatty acids (Fig. 4D). Interestingly, the above regulatory proteins were all enriched in the peroxisome proliferator-activated receptor alpha (PPARα) signaling pathway, suggesting critical regulatory roles for the proteases of the PPARα signaling pathway

in the disruption of fatty acid metabolism during NMBA-induced malignant transformation of Het-1A cells.

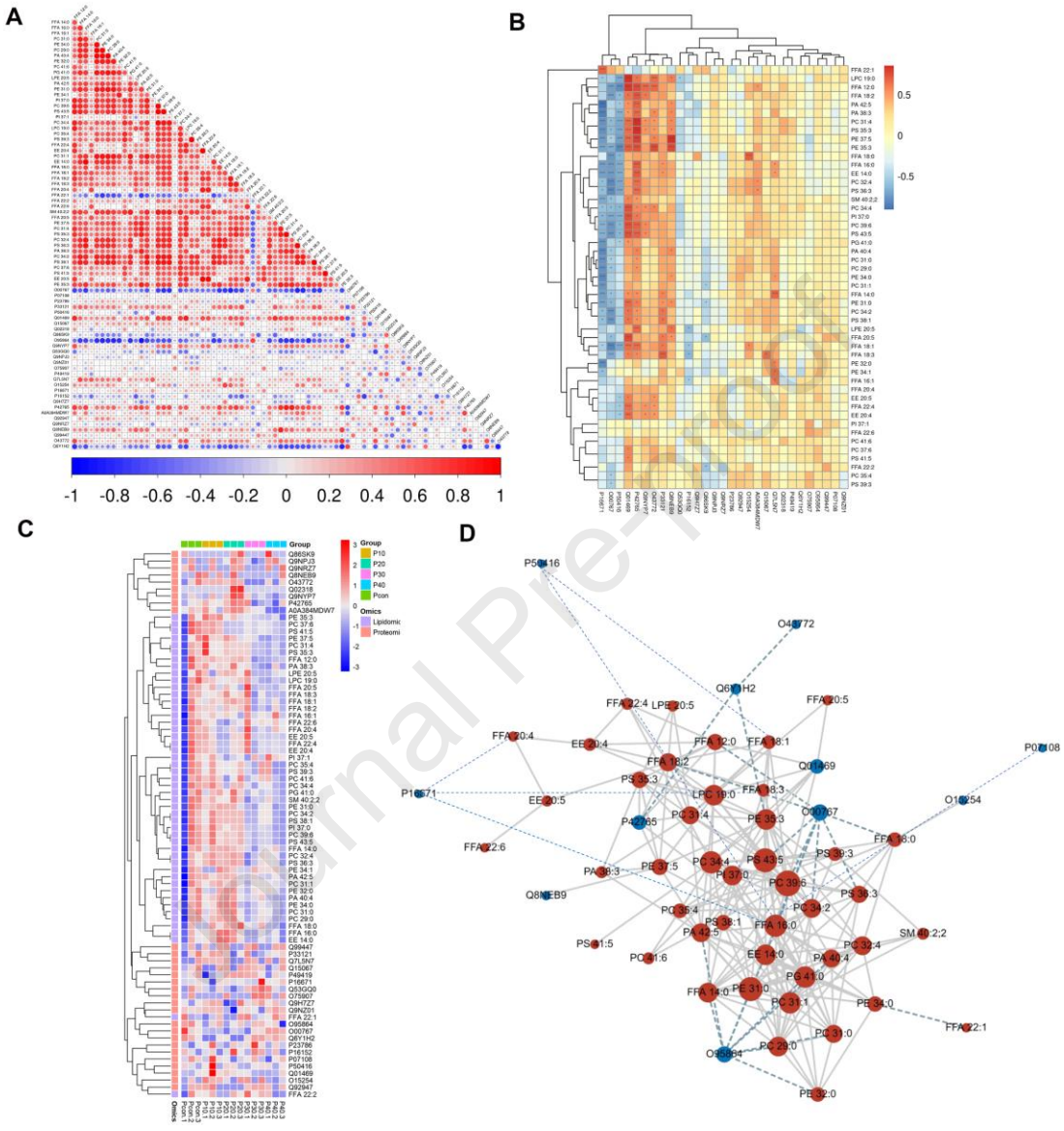

Fig. 4. Integrated analysis of cell proteomics and lipidomics. (A). The cell correlation coefficient matrix heatmap analysis. (B). Spearman correlation hierarchical clustering analysis. (C). The expression of omics clustering heatmap analysis. (D). The correlation analysis network.

3.5 Promotion of fatty acid metabolism involved in the process of cell malignant transformation caused by NMBA

In the PPAR signaling pathway, PPARα facilitated cellular uptake, esterification and transport of fatty acids and regulated lipoprotein genes to stimulate lipid utilization by promoting mitochondrial function and fatty acid desaturation signaling pathways. (Frampton et al., 2020; Montaigne et al., 2021; Wojtowicz et al., 2020). Firstly, we detected the intensities of critical lipid-regulated enzymes, and the levels of SCD, CPT1, ACBP, CD36 showed elevated trend and ACAA2 revealed descending tendency (Fig. 5A). The pivotal gene expression results of PPARα signaling pathway closely related to fatty acid metabolism showed that SCD, PPARα, CD36 and CPT1 were dramatically upregulated in the Pmag cells compared to the control group and ACAA2 expression revealed decreased tendency (Fig. 5B). Also, the western blot analysis exhibited consistent mRNA expression trends of SCD, CPT1, CD36, ACBP, PPARα and ACAA2 levels (Fig. 5C). In addition, the MRM targeted analysis was carried out to quantify the concentrations of key differential FFAs (Table S6 and S7). The quantitative analysis revealed that the concentrations of FFA 12:0, FFA 14:0, FFA 16:1, FFA18:0, FFA 18:1, FFA 18:3, FFA 20:4, FFA 20:5 and FFA 22:6 showed descended tendency accompanied by the increasing generations of Het-1A cells caused by NMBA (Fig.5D). In brief, the activated PPARα signaling pathway exerted important regulatory effects on the fatty acid metabolism in the malignant transformed cells caused by NMBA, and the specific regulatory mechanisms need to be further explored.

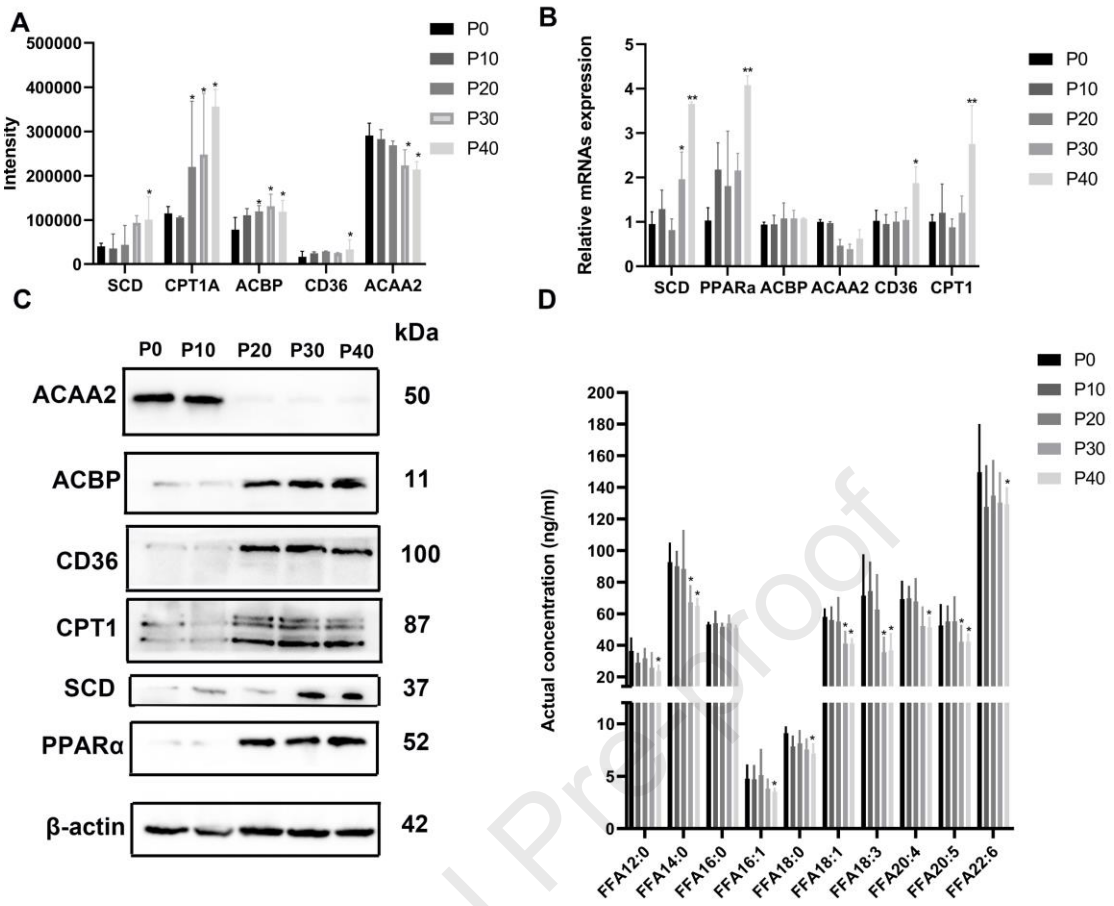

Fig. 5. Enhancement of fatty acid metabolism participated in the process of cell malignant transformation caused by NMBA. (A). The intensities of key lipid-regulated proteases. (B, C). The pivotal gene and protein expression levels of PPARα signaling pathway closely related to fatty acid metabolism in the progression of cell malignant transformation. (D). The FFA concentrations of quantitative MRM targeted analysis. Data were expressed as mean ± SD. $^{**}p < 0.01$, $^{*}p < 0.05$.

3.6. NMBA stimulated esophageal carcinoma tumorigenesis via facilitating PPARα signaling pathway

Accumulating evidence showed that the accelerated oxidation and breakdown of long-chain unsaturated fatty acids were closely associated with the development and progression of carcinomas (Batchuluun et al., 2022; Stine et al., 2022). As the essential role of key genes of PPARα signaling pathway in regulating fatty acid metabolism, we

459 further investigated the regulation effects of PPARα signaling pathway on the malignant
460 transformation phenotype of NMBA-induced Het-1A cells. The pretreatment with
461 critical PPARα pathway inhibitor GW6471 diminished the mRNA and protein levels of
462 SCD, CD36, ACBP, CPT1 and PPARα and elevated the levels of ACAA2 in Pmag cells
463 compared with the control group (Fig. 6A, B). Meanwhile, the protein levels of EMT-
464 signaling malignant progression (E-cadherin, N-cadherin, α-SMA, Snail and Vimentin)
465 were inhibited (Fig. 6C). Compared with the control group, the treating with GW6471
466 suppressed the invasion and migration capacities of Pcon and Pmag cells (Fig. 6D). In
467 addition, the concentrations of key FFAs were strikingly elevated in Pmag cells after
468 pretreated with GW6471, which reversed the changes in these FFAs induced by NMBA
469 (Fig. 6E). Taking together, NMBA exposure induced the tumorigenesis and progression
470 of esophageal cancer through promoting PPARα signaling pathway.

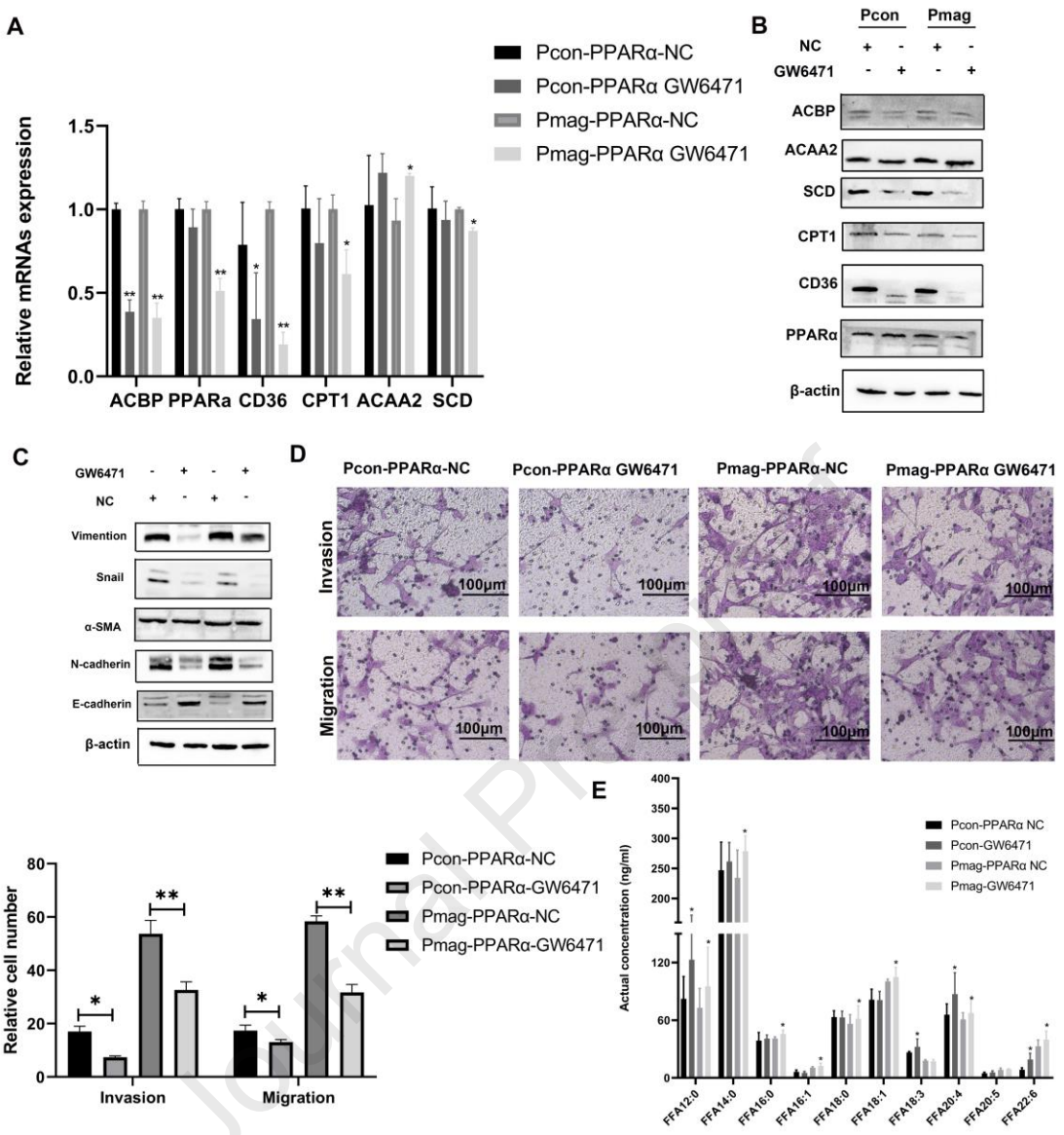

Fig. 6. PPARα signaling pathway-mediated fatty acid metabolism promoted NMBA-induced EC tumorigenesis. (A, B). The mRNA and protein levels of the PPARα signaling pathway (SCD, CD36, CPT1, ACBP, ACAA2, PPARα) were detected by RT–qPCR and western blot analysis after pretreatment with GW6471. (C). The expression levels of EMT pathway proteins (E-cadherin, N-cadherin, α-SMA, Snail and Vimentin). (D). The invasion and migration abilities of Pcon and Pmag cells after inhibition of PPARα expression (bar= 50 μm). (E). The concentrations of key FFAs in Pcon and Pmag cells treating with GW6471. Data were expressed as mean ± SD. $^{**}p < 0.01$, $^{*}p < 0.05$.

3.7. NMBA exposure induced EC tumorigenesis associated with the promotion of fatty acid metabolism in vivo

To validate the results confirmed in vitro, we utilized the control group (C), basal cell hyperplasia stage (L), epithelial dysplasia stage (M) and carcinoma in situ (H) for the progression of NMBA-induced esophageal carcinoma in rats. The mRNAs and protein expression levels of key PPARα pathway regulators related to fatty acid metabolism in esophageal tissues were examined. The results showed that the expression levels of SCD, CD36, PPARα, CPT1, ACBP were remarkably elevated in the H group compared to the C group and ACAA2 revealed declined trend (Fig. 7A, B). Furthermore, the targeted lipidomics analysis showed that the concentrations of FFAs in rat serum samples revealed consistent expression trend in the vitro results, the most FFAs were dramatically decreased in the H group compared with the C group (Fig. 7C). In all, these results further demonstrated that fatty acid metabolism drove the NMBA-induced EC tumorigenesis via regulating PPARα signaling pathway.

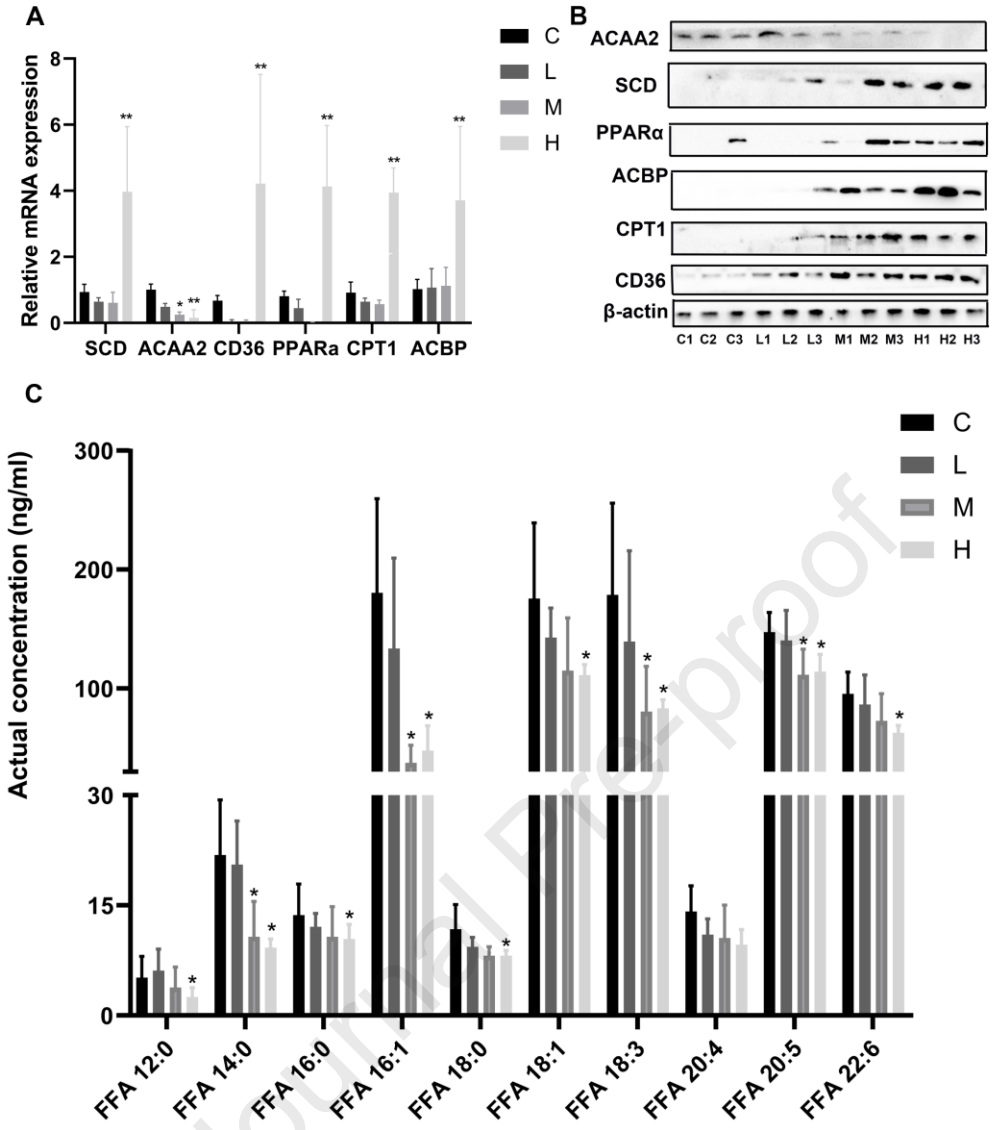

Fig. 7. Environmentally relevant levels of NMBA promoted fatty acid metabolism in vivo. (A, B). The mRNAs and protein expression levels of key regulators in the fatty acid metabolism in the process of NMBA-induced rats esophageal cancer model. (C). The changes in key FFA concentrations of rat serum samples. Data were expressed as mean ± SD. **p < 0.01, *p < 0.05.

4. Discussion

The common environmental carcinogens N-nitrosamines were ubiquitously recognized as important risk factors for EC (Zhao, C. et al., 2019a; Zhao et al., 2020). Carcinogenic N-nitrosamines were catalyzed by cytochrome P450 enzymes to decompose into

aldehydes and hydroxyazo compounds, which caused alkylation damage to DNA and could lead to tumor growth, invasion and metastasis in the esophagus (Li et al., 2022d; Soroush et al., 2022; Zhao et al., 2022). Nevertheless, the molecular mechanisms in the development of N-nitrosamines-induced esophageal carcinogenesis remain largely uncertain. Herein, high-throughput multi-omics-based technology revealed that dysregulation of fatty acid metabolism was involved in NMBA-induced Het-1A cells malignant transformation, while the enhancement of fatty acid metabolism mediated by SCD, CD36, CPT1, and PPARα, key lipid regulators of the PPARα pathway, was closely related to the promotion of NMBA-induced EC phenotype in vitro and vivo studies.

In accordance with the preceding studies, the relative environmental high concentrations of NMBA were set in vitro assays to simulate chronic environmental exposure (Zhang et al., 2022c; Zhao et al., 2020). We observed typical features of the cellular malignant transformation phenotypes at the exposure dose of 2 μM, and NMBA-induced the susceptibility of tumor and tumor-associated protein formation in Het-1A cells was accompanied by an intensification in the degree of malignant transformation. Moreover, to simulate the natural environmental exposure conditions, the rat esophageal cancer model was induced by NMBA exposure. The exposure concentration of NMBA was determined to be 0.4 mg/kg in line with the environmental N-nitrosamine exposure levels (Brown, 2022; Cotruvo, 2017; Zhao et al., 2020), and the molecular mechanism of N-nitrosamines carcinogenesis effect was further explored in vivo and vitro models.

In the current study, the proteomics analysis unveiled lipid metabolism perturbations predominantly participated in the process of NMBA-induced malignant transformation of Het-1A cells. Abundant studies have proven that lipid metabolism destabilization and lipid reprogramming induced by environmental pollutants occurred frequently in carcinomas (Menendez-Pedriza et al., 2022; Wigner et al., 2021), and the cancerous tissues exhibited extensive lipid alteration that led to unrelenting proliferation. Abnormal lipid metabolism profiles were considered to be a hallmark feature of plentiful malignancies (Du et al., 2022; Garofano et al., 2021). Further cell lipidomics analysis showed that fatty acid metabolism and glycerophospholipid metabolism contributed to the predominant dysregulation of lipid profiles. Studies have documented that NMBA could increase lipid peroxidation and free radical production, and the free radicals attacked unsaturated fatty acids in membrane lipids to increase malondialdehyde (MDA) levels (Srinivas et al., 2019). Sphingolipid metabolism-mediated NMBA-induced carcinogenesis in rat esophagus facilitated tumor microenvironment through suppression of immunity functions (Zhao et al., 2022). As indispensable molecules in lipid biosynthesis, FFAs provided substrates for energy-producing metabolism, and the uptake and clearance of extracellular FFAs also proposed crucial compensatory mechanisms for lipid requirements under metabolic stress conditions in cancer cells (Chen et al., 2022; Hou et al., 2022). The critical regulatory implications of fatty acid metabolic alteration in the malignant transformation of cells induced by NMBA need further exploration.

The integration of proteomics and metabolomics detection of immediate metabolites of

protein-coding genes in cells may provide direct evidence to depict complex metabolic changes in cells after exposure to environmental pollutants (Beale et al., 2022; Yang et al., 2022a). In the present study, multi-omics analysis of malignant transformed cells showed remarkably differential lipoprotein enrichment in PPARα signaling pathway and fatty acid metabolism pathways, which uncovered the involvement of fatty acid synthesis (SCD), fatty acid transport (CD36, ACBP) and fatty acid β-oxidative catabolism (CPT1, ACAA2) critical enzymes in the regulation of lipid metabolic profiles during the malignant transformation of NMBA-exposed cells. The consumption of most differential FFA concentrations exhibited accelerated fatty acid metabolism degradation and oxidation during the cells malignant transformation caused by NMBA exposure, accompanying that the expression levels of the critical regulatory enzymes modulating fatty acid metabolism showed upregulation tendency. Exposure to trace heavy metals and antibiotics intervened depletion of long-chain unsaturated fatty acids in zebrafish embryos and caused significant disturbances in immune and tumor-related pathways, indicating a potential risk of tumorigenesis in zebrafish larvae (Jia et al., 2022). Benzo[a]pyrene-induced alteration in fatty acid metabolism, phospholipid metabolism, and sphingolipid metabolism in lung cancer cells were highly affiliated with the invasion and migration of H460 cells (Ye et al., 2021). In brief, the trend of accelerated fatty acid catabolism testified the enhancement of fatty acid metabolism during malignant transformation of NMBA-exposed Het-1A cells, suggesting a close relationship between fatty acid metabolism and esophageal malignant tumorigenesis caused by NMBA.

573 Furthermore, PPARα signaling pathway exerted an increasingly vital function in the
574 regulation of lipid metabolism. The majorities of related genes were involved in the
575 PPARα/CPT1 signaling pathway for fatty acid catabolism, synthesis or transport due to
576 their functional peroxisome response elements (PPREs) (Sheng et al., 2019; Ye et al.,
577 2021). In our results, the activated PPARα signaling pathway accompanied by high
578 expression of SCD, ACBP, CD36 and CPT1, key regulators of fatty acid metabolism,
579 promoted the NMBA-induced malignant transformation phenotypes in Het-1A cells
580 which facilitated esophageal cancer tumorigenesis via promoting the progression of
581 EMT signaling pathway, migration and invasion ability of cells. The SCD inhibitors
582 played a dominant function in primary tumors of cells involved in palmitate-dependent
583 desaturation of alternative pathways (CIS-6-C16:1) that supported membrane synthesis
584 during proliferation and SCD inhibitors could impede the proliferation and invasion of
585 cancer cells in oral cancer (Liu et al., 2022b). CD36 regulated the oxidative
586 decomposition of palmitic acid to facilitate the growth of oral squamous cell carcinoma,
587 and enhanced lipid droplet formation, tumor progression and metastasis (Tao et al.,
588 2022; Bao et al., 2022). Fatty acid oxidation (FAO) was essential for cancer cell survival
589 in various cancers, and CPT1-mediated enhancement in FAO has been noted in
590 numerous malignancies accompanied by the decomposition of acetyl coA (Liu and Liu,
591 2022; Sun et al., 2022). Conversely, the blockade of fatty acid oxidation inhibited tumor
592 growth and CPT1 expression levels in several tumor models (Li et al., 2022a; Ruidas
593 et al., 2022). Exposure to the environmental endocrine disruptor bisphenol A (BPA)
594 during gestation interfered with the expression of the liver fatty acid oxidation-related

595 PPARα and CPT1 and the fatty acid synthesis gene stearoyl coenzyme (SCD) in male
596 offspring (Yang et al., 2022b). Induction of epithelial-mesenchymal transition (EMT)
597 by transforming growth factor β1 (TGF-β1) participated in the metastatic process of
598 breast cancer and caused elevated expression of key fatty acid β-oxidases (CPT1 and
599 CD36) (Liu et al., 2020; Zhao et al., 2021). Consequently, we also investigated the
600 effect of key PPARα pathway inhibitor on NMBA-induced cellular malignant
601 transformation phenotype and free fatty acid levels. The EMT signaling molecules
602 could effectively promote tumor invasion and metastasis, accompanied by the
603 acquisition of an aggressive phenotype when epithelial cells lost their cell-cell adhesion.
604 At the molecular level, the promotion of EMT progression involves increased protein
605 expression levels of Snail, Vimentin, a-SMA and N-cadherin, and decreased level of E-
606 cadherin (Pan et al., 2023; Su et al., 2022). Up to now, there was increasing evidence
607 that N-nitrosamines were vital EMT inducers in lung and bladder cancers, and N-
608 nitrosamines were involved in the bioenergetic reprogramming of cancer cells in
609 concert with alterations in other cancer features such as altered genome and epigenome,
610 dysregulation of cell proliferation and increased migration (Sarlak et al., 2020). Taking
611 together, fatty acid metabolism perturbation contributed to NMBA induced esophageal
612 carcinoma tumorigenesis via regulating PPARα signaling pathway.
613 Disturbances in lipid metabolism induced by environmental pollutants could induce
614 tumorigenesis in the development of cancer, and reprogramming of lipid metabolism
615 played a pivotal role by interfering with energy production, membrane formation and
616 signal transduction in cancer (Bai et al., 2022; Miao et al., 2022). In this study, we

ascertained the specific regulatory mechanisms of impairments of fatty acid metabolism during NMBA exposure-induced EC tumorigenesis. Nevertheless, the relationship between NMBA-induced esophageal malignancy phenotype and specific free fatty acid regulatory mechanisms deserved further comprehensive investigation. Meanwhile, the cell/animal model results should be further validated in the human beings due to the species differences between animals and humans.

5. Conclusion

In summary, the integrated multi-omics analysis revealed the dysregulation lipid metabolism in NMBA exposure triggered esophageal carcinoma tumorigenesis in vitro and vivo. The enhancement of fatty acid metabolism promoted NMBA-induced cell invasion, migratory capacity and EMT progression in the cellular malignant transformation process via regulating the PPARα signaling pathway. To the best of our knowledge, the collective findings propose crucial implications for unraveling the dynamic molecular disorders in NMBA-induced esophageal cancer tumorigenesis and comprehensive elucidation of the adverse health risks of N-nitrosamines.

Declaration of competing interest

The authors declare no competing financial interests or personal relationships that could have appeared to influence the work reported in this study

Acknowledgements

This study was supported by the National Natural Science Foundation of China (No. 81872588, 82073516).

CRediT authorship contribution statement

Hu Zhang: Conceptualization, Software, Data analysis, Writing-Original draft preparation and Editing. **Chao Zhao:** Methodology. **Ying Zhang**: Validation. **Lu Lu**: Visualization. **Wei Shi**: Software. **Qian Zhou:** Conceptualization. **Shizhi Wang**: Supervision. **Ran Liu**: Writing- Reviewing. **Yuepu Pu**: Supervision. **Lihong Yin**: Writing- Reviewing, and Supervision.

Reference:

Abdullah, A.M., Khan, T.A., Sharif, M., Mazumdar, R.M., Rahman, M.M., 2022. Determination of dietary exposure and extraction efficiency of nitrosamine from cooked meat. Current Research in Food Science 5, 491-497.

Bai, Y.S., Cao, Q., Guan, X., Meng, H., Feng, Y., Wang, C.M., Fu, M., Hong, S.R., Zhou, Y.H., Yuan, F.F., Zhang, X.M., He, M.A., Guo, H., 2022. Metabolic linkages between zinc exposure and lung cancer risk: A nested case-control study. Science of the Total Environment 837.

Bao, W., Turniansky, B., Koh, J., 2022. Catalytic covalent inhibition of cyclooxygenase-1 by a biomimetic acyltransferase. Bioorg Med Chem 72, 116973.

Batchuluun, B., Pinkosky, S.L., Steinberg, G.R., 2022. Lipogenesis inhibitors: therapeutic opportunities and challenges. Nature Reviews Drug Discovery 21, 283-305.

Beale, D.J., Sinclair, G.M., Shah, R., Paten, A.M., Kumar, A., Long, S.M., Vardy, S., Jones, O.A.H., 2022. A review of omics-based PFAS exposure studies reveals common biochemical response pathways. Science of the Total Environment 845, 157255.

Boetzel, R., Schlingemann, J., Hickert, S., Korn, C., Kocks, G., Luck, B., Blom, G., Harrison, M., Francois, M., Allain, L., Wu, Y., Bousraf, Y., 2022. A Nitrite Excipient Database: A useful Tool to Support N-Nitrosamine Risk Assessments for Drug Products. J Pharm Sci.

Brown, R., 2022. Updating the WHO Guidelines for drinking-water quality - how are chemicals prioritized? Toxicology Letters 368, S42-S42.

Cai, H., Shen, C., Xu, H., Qian, H., Pei, S., Cai, P., Song, J., Zhang, Y., 2023. Seasonal variability, predictive modeling and health risks of N-nitrosamines in drinking water of Shanghai. Science of the Total Environment 857, 159530.

Chen, W.Q., Zheng, R.S., Baade, P.D., Zhang, S.W., Zeng, H.M., Bray, F., Jemal, A., Yu, X.Q., He, J., 2016. Cancer Statistics in China, 2015. Ca-a Cancer Journal for Clinicians 66, 115-132.

Chen, X., Liu, H., Chen, K., Guo, Y., Mo, T., Gao, T., 2022. Inhibition of autophagy impairs free fatty acid-induced excessive lipid accumulation in hepatocellular carcinoma and hepatic cells. J Biosci 47.

Choi, N.R., Park, S., Ju, S., Kim, E., Kim, S., Choi, N.R., Lim, Y.B., Lee, J.Y., Shine, H.J., Kim, Y.P., 2022. Contribution of liquid water content enhancing aqueous phase reaction forming ambient particulate nitrosamines. Environmental Pollution 303.

677 Cotruvo, J.A., 2017. 2017 WHO Guidelines for Drinking Water Quality: First Addendum to the Fourth
678 Edition. Journal American Water Works Association 109, 44-51.
679 Cui, L., Li, Z., Xu, F., Tian, Y., Chen, T., Li, J., Guo, Y., Lyu, Q., 2022. Antitumor Effects of Astaxanthin
680 on Esophageal Squamous Cell Carcinoma by up-Regulation of PPARgamma. Nutr Cancer 74, 1399-
681 1410.
682 Cui, L.L., Xu, F., Wu, K., Li, L., Qiao, T.Y., Li, Z.L., Chen, T.T., Sun, C.Q., 2020. Anticancer effects and
683 possible mechanisms of lycopene intervention on N-methylbenzylnitrosamine induced esophageal
684 cancer in F344 rats based on PPAR gamma(1). European Journal of Pharmacology 881.
685 Deng, Y.F., Zhang, Y., Ren, H.Q., 2022. Multi-omic studies on the toxicity variations in effluents from
686 different units of reclaimed water treatment. Water Research 208.
687 Dong, L., Jiang, Z.Q., Yang, L.L., Hu, F., Zheng, W.W., Xue, P., Jiang, S.H., Andersen, M.E., He, G.S.,
688 Crabbe, M.J.C., Qu, W.D., 2022. The genotoxic potential of mixed nitrosamines in drinking water
689 involves oxidative stress and Nrf2 activation. Journal of Hazardous Materials 426.
690 Du, D.Y., Liu, C., Qin, M.Y., Zhang, X., Xi, T., Yuan, S.T., Hao, H.P., Xiong, J., 2022. Metabolic
691 dysregulation and emerging therapeutical targets for hepatocellular carcinoma. Acta Pharmaceutica
692 Sinica B 12, 558-580.
693 EPA, 2016. Six-Year Review 3 Technical report Document for Nitrosamines. Office of Water (4607M)
694 EPA 810-R-16-009
695 Ferrer, I., Zweigenbaum, J.A., Thurman, E.M., 2010. Analysis of 70 Environmental Protection Agency
696 priority pharmaceuticals in water by EPA Method 1694. Journal of Chromatography A 1217, 5674-5686.
697 Frampton, J., Murphy, K.G., Frost, G., Chambers, E.S., 2020. Short-chain fatty acids as potential
698 regulators of skeletal muscle metabolism and function. Nature Metabolism 2, 840-848.
699 Gao, M.L., Jiang, Z.B., Liao, X.B., Qi, H., Zhao, L., Chen, C., Westerman, D., 2022. NDMA formation
700 during ozonation of DMAPA: Influencing factors, mechanisms, and new pathway exploration. Science
701 of the Total Environment 825.
702 Garofano, L., Migliozzi, S., Oh, Y.T., D'Angelo, F., Najac, R.D., Ko, A., Frangaj, B., Caruso, F.P., Yu, K.,
703 Yuan, J., Zhao, W., Di Stefano, A.L., Bielle, F., Jiang, T., Sims, P., Suva, M.L., Tang, F., Su, X.D.,
704 Ceccarelli, M., Sanson, M., Lasorella, A., Iavarone, A., 2021. Pathway-based classification of
705 glioblastoma uncovers a mitochondrial subtype with therapeutic vulnerabilities. Cancer Research 81.
706 Hagi, T., Makino, T., Yamasaki, M., Yamashita, K., Tanaka, K., Saito, T., Takahashi, T., Kurokawa, Y.,
707 Motoori, M., Kimura, Y., Nakajima, K., Morii, E., Eguchi, H., Doki, Y., 2022. Pathological Regression
708 of Lymph Nodes Better Predicts Long-term Survival in Esophageal Cancer Patients Undergoing
709 Neoadjuvant Chemotherapy Followed by Surgery. Ann Surg 275, 1121-1129.
710 Hou, H., Chen, D., Zhang, K., Zhang, W., Liu, T., Wang, S., Dai, X., Wang, B., Zhong, W., Cao, H., 2022.
711 Gut microbiota-derived short-chain fatty acids and colorectal cancer: Ready for clinical translation?
712 Cancer Letters 526, 225-235.
713 Hu, C.W., Shih, Y.M., Liu, H.H., Chiang, Y.C., Chen, C.M., Chao, M.R., 2016. Elevated urinary levels
714 of carcinogenic N-nitrosamines in patients with urinary tract infections measured by isotope dilution
715 online SPE LC-MS/MS. Journal of Hazardous Materials 310, 207-216.
716 Jia, D., Zhang, R., Shao, J., Zhang, W., Cai, L., Sun, W., 2022. Exposure to trace levels of metals and
717 fluoroquinolones increases inflammation and tumorigenesis risk of zebrafish embryos. Environ Sci
718 Ecotechnol 10, 100162.
719 Lee, H., Sung, E.J., Seo, S., Min, E.K., Lee, J.Y., Shim, I., Kim, P., Kim, T.Y., Lee, S., Kim, K.T., 2021.
720 Integrated multi-omics analysis reveals the underlying molecular mechanism for developmental

721 neurotoxicity of perfluorooctanesulfonic acid in zebrafish. Environment International 157, 106802.
722 Li, C.L., Zhang, L.L., Qiu, Z.D., Deng, W.H., Wang, W.X., 2022a. Key Molecules of Fatty Acid
723 Metabolism in Gastric Cancer. Biomolecules 12.
724 Li, K.X., Wang, R., Wang, X.X., Sun, C.X., Li, Q., 2022b. Effects of seasons and parts on volatile N-
725 nitrosamines and their exposure and risk assessment in raw chicken and duck meats. Journal of Food
726 Science and Technology-Mysore 59, 1831-1839.
727 Li, R.A., McDonald, J.A., Sathasivan, A., Khan, S.J., 2022c. Multivariate experimental design provides
728 insights for the optimisation of rechloramination conditions and water age to control disinfectant decay
729 and disinfection by-product formation in treated drinking water. Science of the Total Environment 830.
730 Li, X.L., He, X.B., Le, Y., Guo, X.Q., Bryant, M.S., Atrakchi, A.H., McGovern, T.J., Davis-Bruno, K.L.,
731 Keire, D.A., Heflich, R.H., Mei, N., 2022d. Genotoxicity evaluation of nitrosamine impurities using
732 human TK6 cells transduced with cytochrome P450s. Archives of Toxicology 96, 3077-3089.
733 Li, Y.P., Hecht, S.S., 2022. Metabolic Activation and DNA Interactions of Carcinogenic N-Nitrosamines
734 to Which Humans Are Commonly Exposed. International Journal of Molecular Sciences 23.
735 Liao, K.W., Ma, S.J., Liu, C.F., Hu, H.D., Wang, J.F., Wu, B., Ren, H.Q., 2022. High concentrations of
736 dissolved organic nitrogen and N-nitrosodimethylamine precursors in effluent from biological nutrient
737 removal process with low dissolved oxygen conditions. Water Research 216.
738 Lin, K., Shen, Z., Cai, S., Lu, S., 1997. Investigation on nitrosamines in the diets of the inhabitants of
739 high-risk area for esophageal cancer in the southern China and analysis of the correlation factors. Wei
740 Sheng Yan Jiu 26, 266-269.
741 Liu, H.L., Li, G.J., Sturgis, E.M., Shete, S., Dahlstrom, K.R., Du, M.L., Amos, C.I., Christiani, D.C.,
742 Lazarus, P., Wei, Q.Y., 2022a. Genetic variants in CYP2B6 and HSD17B12 associated with risk of
743 squamous cell carcinoma of the head and neck. International Journal of Cancer 151, 553-564.
744 Liu, H.X., Liu, Q.J., 2022. Logistic role of carnitine shuttle system on radiation-induced L-carnitine and
745 acylcarnitines alteration. International Journal of Radiation Biology, 1-14.
746 Liu, Q.Q., Huo, H.Y., Ao, S., Liu, T., Yang, L., Fei, Z.Y., Zhang, Z.Q., Ding, L., Cui, Q.H., Lin, J., Yu,
747 M., Xiong, W., 2020. TGF-beta 1-induced epithelial-mesenchymal transition increases fatty acid
748 oxidation and OXPHOS activity via the p-AMPK pathway in breast cancer cells. Oncology Reports 44,
749 1206-1215.
750 Liu, Y., Liu, X.B., Wang, H., Ding, P.P., Wang, C.L., 2022b. Agrimonolide inhibits cancer progression
751 and induces ferroptosis and apoptosis by targeting SCD1 in ovarian cancer cells. Phytomedicine 101.
752 Lu, S.H., Chui, S.X., Yang, W.X., Hu, X.N., Guo, L.P., Li, F.M., 1991. Relevance of N-nitrosamines to
753 oesophageal cancer in China. Iarc Scientific Publications, 11-17.
754 Luo, H.Y., Lu, J., Bai, Y.X., Mao, T., Wang, J., Fan, Q.X., Zhang, Y.P., Zhao, K.L., Chen, Z.D., Gao, S.G.,
755 Li, J.C., Fu, Z.C., Gu, K.S., Liu, Z.H., Wu, L., Zhang, X.D., Feng, J.F., Niu, Z.X., Ba, Y., Zhang, H.L.,
756 Liu, Y., Zhang, L., Min, X.H., Huang, J., Cheng, Y., Wang, D., Shen, Y., Yang, Q., Zou, J.J., Xu, R.H.,
757 Investigators, E.-s., 2021. Effect of Camrelizumab vs Placebo Added to Chemotherapy on Survival and
758 Progression-Free Survival in Patients With Advanced or Metastatic Esophageal Squamous Cell
759 Carcinoma: The ESCORT-1st Randomized Clinical Trial. Jama-Journal of the American Medical
760 Association 326, 916-925.
761 Lyon, A.S., Peeples, W.B., Rosen, M.K., 2021. A framework for understanding the functions of
762 biomolecular condensates across scales. Nature Reviews Molecular Cell Biology 22, 215-235.
763 Maqbool, T., Zhang, J.X., Li, Q.Y., Qin, Y.L., Chen, L., Zhang, Z.H., 2021. Occurrence and fate of N-
764 nitrosamines in three full-scale drinking water treatment systems with different treatment trains. Science

765 of the Total Environment 783.
766 Menendez-Pedriza, A., Jaumot, J., Bedia, C., 2022. Lipidomic analysis of single and combined effects
767 of polyethylene microplastics and polychlorinated biphenyls on human hepatoma cells. Journal of
768 Hazardous Materials 421.
769 Molina-Aguilar, C., Arriaga-Gonzalez, F., Castaneda, F., Villa-Malagon, K., Simonin-Wilmer, I.,
770 Sanchez, O.R., Garza, E.C., Azuara, M.L., Juarez, O.L., Velasco-Herrera, M.D., Adams, D., Diaz-Munoz,
771 M., Robles-Espinoza, C.D., 2022. The protective effect of time-caloric restriction in liver fibrosis
772 induced by nitrosamines in rat model. Journal of Hepatology 77, S476-S476.
773 Montaigne, D., Butruille, L., Staels, B., 2021. PPAR control of metabolism and cardiovascular functions.
774 Nature Reviews Cardiology 18, 809-823.
775 Pan, C., Qin, H.X., Yan, M.H., Qiu, X.F., Gong, W.Y., Luo, W.X., Guo, H.Q., Han, X.D., 2023.
776 Environmental microcystin exposure triggers the poor prognosis of prostate cancer: Evidence from case-
777 control, animal, and in vitro studies. Journal of Environmental Sciences 127, 69-81.
778 Pan, F., Chen, Y., He, J.Z., Long, L., Chen, Y., Luo, H.J., Xu, Y.W., Pang, X.X., Yang, Q., Wang, J.J., Xu,
779 X.E., Wang, S.H., Li, E.M., Xu, L.Y., 2019. Dietary riboflavin deficiency promotes N-
780 nitrosomethylbenzylamine-induced esophageal tumorigenesis in rats by inducing chronic inflammation.
781 American Journal of Cancer Research 9, 2469-2481.
782 Qiu, Y., Bei, E., Li, X., Xie, S.G., Xiao, H., Luo, Y.H., Wang, Y., Wang, J., Zhang, X.J., Chen, C., 2021.
783 Quantitative analysis of source and fate of N-nitrosamines and their precursors in an urban water system
784 in East China. Journal of Hazardous Materials 415.
785 Ruidas, B., Sur, T.K., Das Mukhopadhyay, C., Sinha, K., Chaudhury, S.S., Sharma, P., Bhowmick, S.,
786 Majumder, R., Saha, A., 2022. Quercetin: a silent retarder of fatty acid oxidation in breast cancer
787 metastasis through steering of mitochondrial CPT1. Breast Cancer 29, 748-760.
788 Sambiagio, N., Berthet, A., Wild, P., Sauvain, J.J., Auer, R., Schoeni, A., Rodondi, N., Feller, M., Humair,
789 J.P., Berlin, I., Breider, F., Grandjean, D., Hopf, N.B., 2022. Associations between urinary biomarkers of
790 oxidative stress and biomarkers of tobacco smoke exposure in smokers. Science of the Total Environment
791 852, 158361.
792 Sarlak, S., Lalou, C., Amoedo, N.D., Rossignol, R., 2020. Metabolic reprogramming by tobacco-specific
793 nitrosamines (TSNAs) in cancer. Seminars in Cell & Developmental Biology 98, 154-166.
794 Shen, Y., Xie, G., Lin, S., Zhu, L., Zhang, H., Yang, Z., Cai, Z., 2022. Metabolomics and proteomics
795 study reveals the effects of benzo[a]pyrene on the viability and migration of KYSE-150 esophageal cells.
796 Science of the Total Environment 824, 153761.
797 Sheng, D., Zhao, S., Gao, L., Zheng, H., Liu, W., Hou, J., Jin, Y., Ye, F., Zhao, Q., Li, R., Zhao, N., Zhang,
798 L., Han, Z., Wei, L., 2019. BabaoDan attenuates high-fat diet-induced non-alcoholic fatty liver disease
799 via activation of AMPK signaling. Cell Biosci 9, 77.
800 Soroush, A., Etemadi, A., Abrams, J.A., 2022. Non-Acid Fluid Exposure and Esophageal Squamous Cell
801 Carcinoma. Digestive Diseases and Sciences 67, 2754-2762.
802 Srinivas, U.S., Tan, B.W.Q., Vellayappan, B.A., Jeyasekharan, A.D., 2019. ROS and the DNA damage
803 response in cancer. Redox Biology 25, 101084.
804 Stine, Z.E., Schug, Z.T., Salvino, J.M., Dang, C.V., 2022. Targeting cancer metabolism in the era of
805 precision oncology. Nature Reviews Drug Discovery 21, 141-162.
806 Su, S.H., Sundhar, N., Kuo, W.W., Lai, S.C., Kuo, C.H., Ho, T.J., Lin, P.Y., Lin, S.Z., Shih, C.Y., Lin,
807 Y.J., Huang, C.Y., 2022. Artemisia argyi extract induces apoptosis in human gemcitabine-resistant lung
808 cancer cells via the PI3K/MAPK signaling pathway. Journal of Ethnopharmacology 299.

Sun, Y., Guo, W., Guo, Y., Lin, Z., Wang, D., Guo, Q., Zhou, Y., 2022. Apoptosis induction in human prostate cancer cells related to the fatty acid metabolism by wogonin-mediated regulation of the AKT-SREBP1-FASN signaling network. Food and Chemical Toxicology 169, 113450.

Sung, H., Ferlay, J., Siegel, R.L., Laversanne, M., Soerjomataram, I., Jemal, A., Bray, F., 2021. Global cancer statistics 2020: GLOBOCAN estimates of incidence and mortality worldwide for 36 cancers in 185 countries. Ca-a Cancer Journal for Clinicians 71, 209-249.

Tang, X., Benowitz, N., Gundel, L., Hang, B., Havel, C.M., Hoh, E., Jacob Iii, P., Mao, J.H., Martins-Green, M., Matt, G.E., Quintana, P.J.E., Russell, M.L., Sarker, A., Schick, S.F., Snijders, A.M., Destaillats, H., 2022. Thirdhand Exposures to Tobacco-Specific Nitrosamines through Inhalation, Dust Ingestion, Dermal Uptake, and Epidermal Chemistry. Environmental Science & Technology 56, 12506-12516.

Tao, L.D., Ding, X.M., Yan, L.L., Xu, G.C., Zhang, P.J., Ji, A.L., Zhang, L.H., 2022. CD36 accelerates the progression of hepatocellular carcinoma by promoting FAs absorption. Medical Oncology 39.

Trejo-Martin, A., Bercu, J.P., Thresher, A., Tennant, R.E., Thomas, R.F., Cross, K., Czich, A., Waese, K., Nicolette, J.J., Murray, J., Sonders, P., Kondratiuk, A., Cheung, J.R., Thomas, D., Lynch, A., Harvey, J., Glowienke, S., Custer, L., Escobar, P.A., 2022. Use of the bacterial reverse mutation assay to predict carcinogenicity of N-nitrosamines. Regul Toxicol Pharmacol 135, 105247.

Vogel, M., Norwig, J., 2022. Analysis of genotoxic N-nitrosamines in active pharmaceutical ingredients and market authorized products in low abundance by means of liquid chromatography - tandem mass spectrometry. J Pharm Biomed Anal 219, 114910.

Wigner, P., Grebowski, R., Bijak, M., Saluk-Bijak, J., Szemraj, J., 2021. The Interplay between Oxidative Stress, Inflammation and Angiogenesis in Bladder Cancer Development. International Journal of Molecular Sciences 22.

Wojtowicz, S., Strosznajder, A.K., Jezyna, M., Strosznajder, J.B., 2020. The Novel Role of PPAR Alpha in the Brain: Promising Target in Therapy of Alzheimer's Disease and Other Neurodegenerative Disorders. Neurochemical Research 45, 972-988.

Xia, C., Dong, X., Li, H., Cao, M., Sun, D., He, S., Yang, F., Yan, X., Zhang, S., Li, N., Chen, W., 2022. Cancer statistics in China and United States, 2022: profiles, trends, and determinants. Chin Med J (Engl) 135, 584-590.

Xu, L., Zhao, Q., Luo, J., Ma, W., Jin, Y., Li, C., Hou, Y., Feng, M., Wang, Y., Chen, J., Zhao, J., Zheng, Y., Yu, D., 2020. Integration of proteomics, lipidomics, and metabolomics reveals novel metabolic mechanisms underlying N, N-dimethylformamide induced hepatotoxicity. Ecotoxicol Environ Saf 205, 111166.

Yan, L., Chen, S., Hou, C., Lin, J., Xiong, W., Shen, Y., Zhou, T., 2022. Multi-omics analysis unravels dysregulated lysosomal function and lipid metabolism involved in sub-chronic particulate matter-induced pulmonary injury. Science of the Total Environment 836, 155642.

Yang, H., Jia, X.D., Chen, X.X., Yang, C.S., Li, N., 2012. Time-selective chemoprevention of vitamin E and selenium on esophageal carcinogenesis in rats: The possible role of nuclear factor kappaB signaling pathway. International Journal of Cancer 131, 1517-1527.

Yang, Y., Wang, H., Wang, X.Y., Chen, L., Liu, W.Y., Cai, D.P., Deng, S.X., Chu, H.Y., Liu, Y., Feng, X.L., Chen, J.H., Chen, M.S., Wang, C.K., Liu, R., Pu, Y.P., Ding, Z., Cao, D.L., Long, D.X., Cao, Y., Yang, F., 2022a. Long-term environmental levels of microcystin-LR exposure induces colorectal chronic inflammation, fibrosis and barrier disruption via CSF1R/ Rap1b signaling pathway. Journal of Hazardous Materials 440.

Yang, Q., Mao, Y., Wang, J., Yu, H., Zhang, X., Pei, X., Duan, Z., Xiao, C., Ma, M., 2022b. Gestational bisphenol A exposure impairs hepatic lipid metabolism by altering mTOR/CRTC2/SREBP1 in male rat offspring. Human & Experimental Toxicology 41.

Yang, W., Cortijo, S., Korsbo, N., Roszak, P., Schiessl, K., Gurzadyan, A., Wightman, R., Jonsson, H., Meyerowitz, E., 2021. Molecular mechanism of cytokinin-activated cell division in Arabidopsis. Science 371, 1350-1355.

Ye, G.Z., Gao, H., Wu, Z.M., Chen, J.S., Zhang, J., Huang, Q.S., 2021. Comprehensive metabolomics insights into benzo[a]pyrene-induced metabolic reprogramming related to H460 cell invasion and migration. Science of the Total Environment 774.

Zhang, X.L., Kim, D., Freedman, D.L., Karanfil, T., 2020. Source characterization and removal ofN-nitrosamine precursors during activated sludge treatment. Environmental Science-Water Research & Technology 6, 2432-2443.

Zhang, Q., Du, X., Li, H., Jiang, Y., Zhu, X., Zhang, Y., Niu, Y., Liu, C., Ji, J., Chillrud, S.N., Cai, J., Chen, R., Kan, H., 2022a. Cardiovascular effects of traffic-related air pollution: A multi-omics analysis from a randomized, crossover trial. Journal of Hazardous Materials 435, 129031.

Zhang, H., Liu, Q.W., Zhao, C., Zhang, Y., Wang, S.Z., Liu, R., Pu, Y.P., Yin, L.H., 2022b. The dysregulation of unsaturated fatty acid-based metabolomics in the MNNG-induced malignant transformation of Het-1A cells. Environmental Science and Pollution Research 29, 30159-30168.

Zhang, H., Lu, L., Zhao, C., Liu, Q., Zhou, Q., Zhang, Y., Pu, Y., Wang, S., Liu, R., Yin, L., 2022c. Lipid metabolism disorders contribute to hepatotoxicity of ICR mice induced by nitrosamines exposure. Environment International 167, 107423.

Zhang, H., Zhao, C., Liu, Q., Zhang, Y., Luo, K., Pu, Y., Yin, L., 2022d. Dysregulation of fatty acid metabolism associated with esophageal inflammation of ICR mice induced by nitrosamines exposure. Environmental Pollution 297, 118680.

Zhao, C., Lu, Q., Gu, Y., Pan, E.C., Sun, Z.M., Zhang, H., Zhou, J.J., Du, Y., Zhang, Y., Feng, Y.M., Liu, R., Pu, Y.P., Yin, L.H., 2019a. Distribution of N-nitrosamines in drinking water and human urinary excretions in high incidence area of esophageal cancer in Huai'an, China. Chemosphere 235, 288-296.

Zhao, C., Zhang, H., Zhou, J., Liu, Q., Lu, Q., Zhang, Y., Yu, X., Wang, S., Liu, R., Pu, Y., Yin, L., 2022. Metabolomic transition trajectory and potential mechanisms of N-nitrosomethylbenzylamine induced esophageal squamous cell carcinoma in rats. Ecotoxicology and Environmental Safety 244, 114071.

Zhao, C., Zhou, J., Gu, Y., Pan, E., Sun, Z., Zhang, H., Lu, Q., Zhang, Y., Yu, X., Liu, R., Pu, Y., Yin, L., 2020. Urinary exposure of N-nitrosamines and associated risk of esophageal cancer in a high incidence area in China. Science of the Total Environment 738, 139713.

Zhao, C.S., Wei, W., Luo, S.W., Yang, P., Ren, Y.H., Liu, Y., Wang, W.N., 2021. FABP regulates fatty acid metabolism and oxidative response via PPAR alpha/RXR signaling in Litopenaeus vannamei following environmental exposure of clofibric acid. Ecotoxicology 30, 954-965.

Zhao, L., Li, Y.C., Wu, J.P., Zhao, Y.J., Wang, R.B., Jiang, M., Song, Q.K., 2019b. Increased risk of esophageal squamous cell carcinoma associated with frequent and long-term consumption of salted meat and salted fat. Journal of International Medical Research 47, 3841-3849.

Highlights

. NMBA exposure caused Het-1A cells malignant transformation and tumorigenesis

. Lipid metabolism disorder involved in the process of malignant cells induced by NMBA.

. Promotion of fatty acid metabolism contributed to the process of NMBA triggered EC.

. NMBA stimulated EC tumorigenesis via PPARα signaling pathway in vitro and vivo.

Declaration of interests

☒ The authors declare that they have no known competing financial interests or personal relationships that could have appeared to influence the work reported in this paper.

☐The authors declare the following financial interests/personal relationships which may be considered as potential competing interests: